Computers and Concrete, Vol. 2, No. 4 (2005) 309-324
DOI: http://dx.doi.org/10.12989/cac.2005.2.4.309

Complete moment-curvature relationship of reinforced normal- and high-strength concrete beams experiencing complex load history

F. T. K. Au†, B. Z. Z. Bai‡ and A. K. H. Kwan‡†

Department of Civil Engineering, The University of Hong Kong, Pokfulam Road, Hong Kong, P.R. China

(Received October 23, 2004, Accepted August 7, 2005)

Abstract. The moment-curvature relationship of reinforced concrete beams made of normal- and high-strength concrete experiencing complex load history is studied using a numerical method that employs the actual stress-strain curves of the constitutive materials and takes into account the stress-path dependence of the concrete and steel reinforcement. The load history considered includes loading, unloading and reloading. From the results obtained, it is found that the complete moment-curvature relationship, which is also path-dependent, is similar to the material stress-strain relationship with stress-path dependence. However, the unloading part of the moment-curvature relationship of the beam section is elastic but not perfectly linear, although the unloading of both concrete and steel is assumed to be linearly elastic. It is also observed that when unloading happens, the variation of neutral axis depth has different trends for under- and over-reinforced sections. Moreover, even when the section is fully unloaded, there are still residual curvature and stress in the section in some circumstances. Various issues related to the post-peak behavior of reinforced concrete beams are also discussed.

Keywords: high-strength concrete; moment-curvature relationship; normal-strength concrete; reinforced concrete beams; stress-path dependence; unloading and reloading.

1. Introduction

In the design of structures, both strength and ductility are important for structural safety. Very often the strength aspect is given much attention while it is simply assumed that the design code used will provide a certain minimum level of ductility to avoid brittle failure. With the increasing use of high-strength concrete (ACI Committee 363, 1992) that is inherently more brittle than normal-strength concrete, engineers have started to pay more attention to the ductility and complete flexural behavior of reinforced concrete (RC) beams made with such materials. To accurately assess the safety of a structure, a full-range analysis to obtain the behavior of both the pre-peak and post-peak stages is necessary. Carreira and Chu (1986) presents a general non-linear method to compute the moment-curvature relationship of RC members. A numerical method for the full-range moment-curvature analysis of RC beams under monotonic increase of curvature, which takes into account

† Associate Professor, E-mail: francis.au@hku.hk
‡ PhD Student
‡† Professor and Associate Dean

the non-linear stress-strain relationship and stress-path dependence of the constitutive materials, has been developed and applied to rectangular beams (Pam, *et al*. 2001) and flanged beams (Au and Kwan 2004, Kwan and Au 2004). Consider an RC beam on which the deformations at certain sections are imposed monotonically. Normally a plastic hinge will sooner or later form at a loaded section, where the curvature and deflection increase monotonically as well. The bending moment there increases accordingly until it reaches the peak strength, after which it drops gradually until the structure completely collapses. However the equilibrium of the beam requires that the other sections not directly loaded will experience unloading and consequently curvature reversal without reaching their respective peak moments. Therefore even in a structure that is loaded monotonically, some parts of it may experience curvature reversal, not to mention the much more complex load history imposed by earthquakes.

A few investigators have studied the behavior of reinforced concrete beams under complex loading typical of seismic motions. Kent and Park (1971) investigated experimentally and theoretically the inelastic behavior of reinforced concrete members under cyclic loading, which were made of normal-strength concrete and mild steel reinforcement. In particular, they studied the Bauschinger effect for cyclically stressed mild steel reinforcement and the influence of rectangular steel hooping on the stress-strain behavior of concrete. Brown and Jirsa (1971) carried out experiments on RC cantilever beams and investigated the effect of load history on the strength, ductility, and mode of failure. They concluded that the behavior of the specimens under load reversal was influenced primarily by shear.

This paper describes a new method of full-range moment-curvature analysis of RC beams experiencing complex load history. It employs the actual stress-strain curves of the constitutive materials and takes into account the stress-path dependence of the concrete and steel reinforcement. The method is applied to the full-range analysis of RC beam sections to study their complete moment-curvature relationship.

2. Stress-strain relationship of concrete with stress-path dependence

In the present study, the stress-strain curve of concrete developed by Attard and Setunge (1996), which has been shown to be applicable to a broad range of *in situ* concrete strength from 20 to 130 MPa, is employed. In this model, the parameters used to establish the stress-strain curve are the initial Young's modulus E_c, the peak stress f_{co} and the corresponding strain ε_{co}, and the stress f_{ci} and strain ε_{ci} at the inflection point on the descending branch of the curve. The stress of concrete σ_c is related to the strain ε_c by

$$\sigma_c/f_{co} = \frac{A(\varepsilon_c/\varepsilon_{co}) + B(\varepsilon_c/\varepsilon_{co})^2}{1 + (A-2)(\varepsilon_c/\varepsilon_{co}) + (B+1)(\varepsilon_c/\varepsilon_{co})^2} \tag{1}$$

where A and B are coefficients dependent on the concrete grade. Two sets of the coefficients A and B are required, one for the ascending branch and another for the descending branch of the curve. For the ascending branch where $\varepsilon \leq \varepsilon_{co}$,

$$A = \frac{E_c \varepsilon_{co}}{f_{co}}; \quad B = \frac{(A-1)^2}{0.55} - 1 \tag{2}$$

For the descending branch where $\varepsilon > \varepsilon_{co}$,

$$A = \frac{f_{ci}(\varepsilon_{ci} - \varepsilon_{co})^2}{\varepsilon_{co}\varepsilon_{ci}(f_{co} - f_{ci})}; \qquad B = 0 \tag{3}$$

The parameters E_c, ε_{co}, f_{ci} and ε_{ci} are related to the peak stress f_{co} by

$$E_c = 4370(f_{co})^{0.52} \tag{4a}$$

$$\varepsilon_{co} = 4.11(f_{co})^{0.75}/E_c \tag{4b}$$

$$\frac{f_{ci}}{f_{co}} = 1.41 - 0.17\ \ln(f_{co}) \tag{4c}$$

$$\frac{\varepsilon_{ci}}{\varepsilon_{co}} = 2.50 - 0.30\ \ln(f_{co}) \tag{4d}$$

It should be noted that the peak stress f_{co} is actually the *in situ* uniaxial compressive strength of concrete, which may be determined from the standard cube or cylinder strengths using appropriate correction factors. Fig. 1(a) shows the parameters used to define a stress-strain curve using this model, while some typical stress-strain curves for *in situ* concrete strength from 40 to 100 MPa are shown in Fig. 1(b). To cope with the unloading and reloading in the material, the stress-path dependence of the stress-strain relation is taken into account. The unloading is treated as linearly elastic (Bangash 2001), as shown in Fig. 2(a). The point from which unloading starts has to be stored for subsequent computations. For example, unloading from point 2 in Fig. 2(a) follows the straight line 2-1 that is parallel to the tangent to the stress-strain curve at the origin. Reloading from point 1 then follows the path 1-2-3, which comprises the straight line 1-2 and the original curve 2-3. During unloading and reloading along path 1-2, the stress σ_c is related to the strain ε_c by

$$\sigma_c = E_c(\varepsilon_c - \varepsilon_{pc}) \tag{5}$$

where E_c is the initial tangent modulus and ε_{pc} is the residual strain of the path.

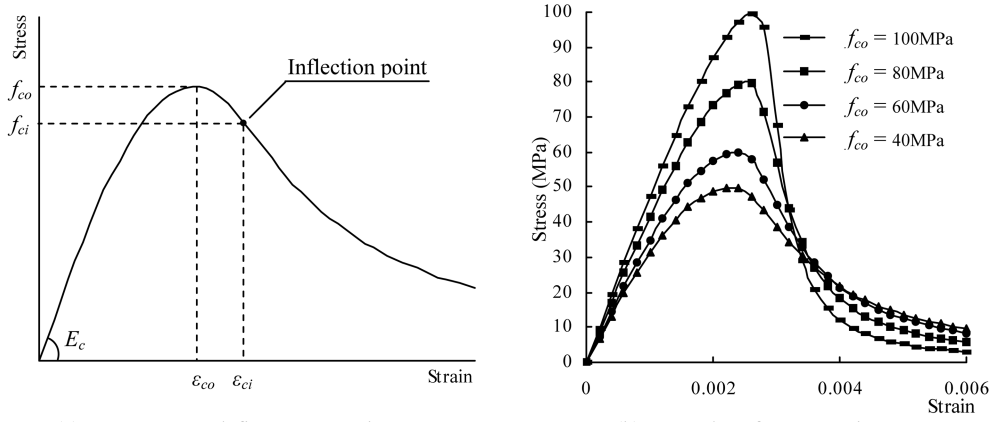

(a) Parameters to define stress-strain curve (b) Examples of stress-strain curves

Fig. 1 Stress-strain curves of concrete according to the Attard-Setunge Model

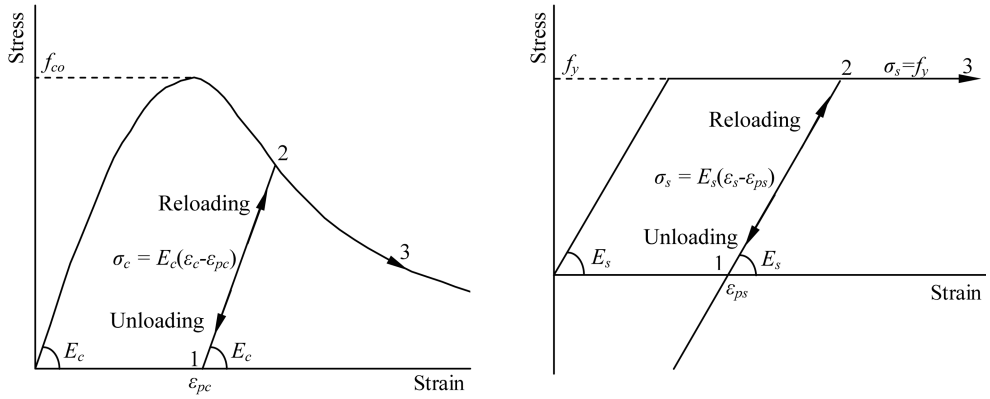

Fig. 2 Stress-strain curves of material constituents with stress path dependence

3. Stress-strain relationship of steel with stress-path dependence

A linearly elastic-perfectly plastic stress-strain model as shown in Fig. 2(b) is used for the steel reinforcement. When the strain ε_s is increasing, the stress σ_s in the steel is given by

$$\text{at elastic stage: } \sigma_s = E_s\varepsilon_s \text{ for } \varepsilon_s \leq f_y/E_s \tag{6a}$$

$$\text{after yielding: } \sigma_s = f_y \text{ for } \varepsilon_s > f_y/E_s \tag{6b}$$

where E_s is the Young's modulus and f_y is the yield stress. It is assumed that unloading from a typical point 2 on the yielding plateau in Fig. 2(b) follows the straight line 2-1 following the initial elastic slope. Reloading from point 1 then follows the path 1-2-3. The stress σ_s and the strain ε_s along path 1-2 are related by

$$\sigma_s = E_s(\varepsilon_s - \varepsilon_{ps}) \tag{7}$$

where ε_{ps} is the residual strain of path 1-2.

4. Non-linear analysis method

The three basic assumptions made in the analysis are (a) plane sections before bending remain plane after bending; (b) tensile stress in the concrete may be neglected; and (c) there is no bond-slip between the reinforcement bars and the concrete. They imply that the longitudinal strains developed at various points of a section are proportional to the distances from the neutral axis. They are commonly accepted and are nearly exact except in deep beams or in the vicinity of cracks. Fig. 3 shows a beam section having a breadth b and total depth h, with the tension reinforcement area A_{st} provided at a depth d and the compression reinforcement area A_{sc} provided at a depth d_1 from the top. For convenience in analysis, the sign convention adopted is such that the strain and stress quantities are normally positive as follows: (a) compressive strain and stress in concrete are

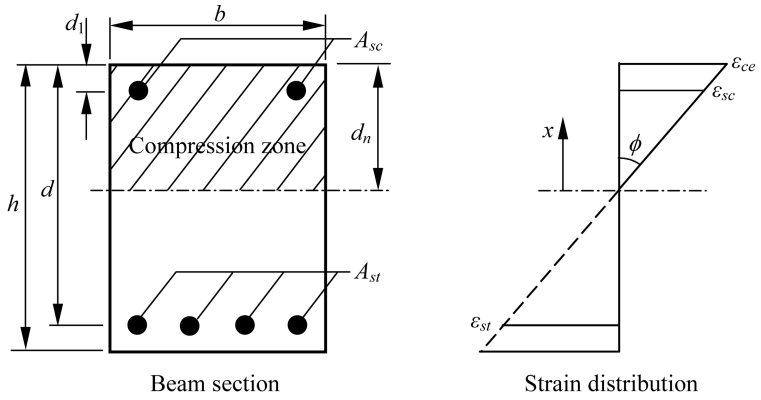

Fig. 3 A beam section subjected to bending moment

positive; (b) compressive strain and stress in compression reinforcement are positive; and (c) tension strain and stress in the tension reinforcement are positive. When the curvature of the beam section is increased to f as shown in the strain distribution diagram in Fig. 3, the strain ε developed is given by

$$\varepsilon = \phi x \tag{8}$$

where x is the distance above the neutral axis. Therefore, the compressive strain ε_{ce} at the extreme concrete compression fiber, the compressive strain ε_{sc} in the compression reinforcement and the tensile strain ε_{st} in the tension reinforcement can be respectively written as

$$\varepsilon_{ce} = \phi d_n \tag{9a}$$

$$\varepsilon_{sc} = \phi(d_n - d_1) \tag{9b}$$

$$\varepsilon_{st} = \phi(d - d_n) \tag{9c}$$

in which d_n is the neutral axis depth. The corresponding stresses σ_c, σ_{sc} and σ_{st} developed in the concrete, compression reinforcement and tension reinforcement can then be evaluated from the respective stress-strain curves of the materials taking into account stress path dependence. To cater for the subsequent unloading and reloading, the latest residual strains ε_{pc} of the concrete section, ε_{pc} of the tension reinforcement and the compression reinforcement should be stored and updated. The residual strains ε_{pc} of the concrete section at regular intervals along the depth are recorded so that the values at intermediate positions can be obtained by linear interpolation.

The stresses developed in the beam section must satisfy the conditions of axial equilibrium and moment equilibrium. The applied axial load P can be obtained from axial equilibrium as

$$P = \int_0^{d_n} \sigma_c b dx + \sum A_{sc}\sigma_{sc} - \sum A_{st}\sigma_{st} = 0 \tag{10}$$

where compressive force is taken as positive. Similarly, the resisting moment M can be obtained from moment equilibrium as

$$M = \int_0^{d_n} \sigma_c b x dx + \sum A_{sc}\sigma_{sc}(d_n - d_1) + \sum A_{st}\sigma_{st}(d - d_n) \tag{11}$$

where sagging moment is taken as positive. In the evaluation of integrals in Eqs. (10) and (11), Romberg integration (Gerald and Wheatley 1999), which can significantly improve the accuracy of the simple trapezoidal rule when the integrand is known at equispaced intervals, has been adopted. The axial equilibrium condition as shown in Eq. (10) can be used to determine the neutral axis depth d_n. Normally, given a specified curvature ϕ and a trial value of neutral axis depth d_n, the equilibrium condition is not immediately satisfied and there is an unbalanced axial force P. Since the relation between the unbalanced axial force P and the neutral axis depth d_n is nonlinear, an iterative scheme is required to determine the value of d_n which will give a zero value of P. The scheme adopted here is the modified linear interpolation method (Gerald and Wheatley 1999).

The complete moment-curvature relationship including loading, unloading and reloading is then obtained through a prescribed variation of curvature by a suitable step size. The curvature ϕ increases gradually from zero to a certain curvature ϕ_1, from which unloading takes place with the curvature ϕ gradually decreases until the resisting moment of the section is close to zero. This is then followed by reloading so that the curvature ϕ gradually increases until it reaches a curvature ϕ_2 that is larger than ϕ_1, from which unloading takes place again. This is repeated until the maximum resisting moment upon reloading has dropped to a small enough value compared with the overall peak resisting moment.

5. Results of analysis

5.1. Sections analyzed

The beam sections analyzed are rectangle in shape as shown in Fig. 3. A typical beam section has a breadth b = 300 mm and total depth h = 600 mm, with the tension reinforcement provided at a depth d = 550 mm and the compression reinforcement provided at a depth d_1 = 50 mm from the top.

Table 1 Cases investigated

f_{co} (MPa)	ρ_c (%)	ρ_b (%)	ρ_t (%)	Remarks
30	0	3.19	1.60	Under-reinforced
	0	3.19	4.79	Over-reinforced
	1	4.19	2.10	Under-reinforced
	1	4.19	6.29	Over-reinforced
60	0	5.39	2.70	Under-reinforced
	0	5.39	8.09	Over-reinforced
	1	6.39	3.20	Under-reinforced
	1	6.39	9.59	Over-reinforced
90	0	7.30	3.65	Under-reinforced
	0	7.30	10.95	Over-reinforced
	1	8.30	4.15	Under-reinforced
	1	8.30	12.45	Over-reinforced

The steel reinforcement has a yield strength f_y = 460 MPa and Young's modulus E_s = 200 GPa. Altogether twelve cases have been investigated as shown in Table 1. The *in situ* concrete compressive strength f_{co} ranges from 30 to 90 MPa to cover both normal- and high-strength concrete. The beam sections may be singly or doubly reinforced with the compression steel ratio ρ_c ($\rho_c = A_{sc}/bd$) up to 1%. The tension steel is provided with respect to the balanced steel ratio ρ_b so as to cover both under- and over-reinforced cases. The tension steel ratio ρ_t ($\rho_t = A_{st}/bd$) varies from $0.5\rho_b$ to $1.5\rho_b$.

5.2. Complete moment-curvature relationship of beam sections experiencing complex load history

Fig. 4 shows the complete moment-curvature relationship of sections with *in situ* concrete compressive strength f_{co} of 30 MPa, while Fig. 5 shows those for 90 MPa. The solid lines represent the response under monotonic loading (i.e. increase in curvature) whereas the dash lines denote the response on unloading (i.e. decrease in curvature) and reloading. It is found that, under the present

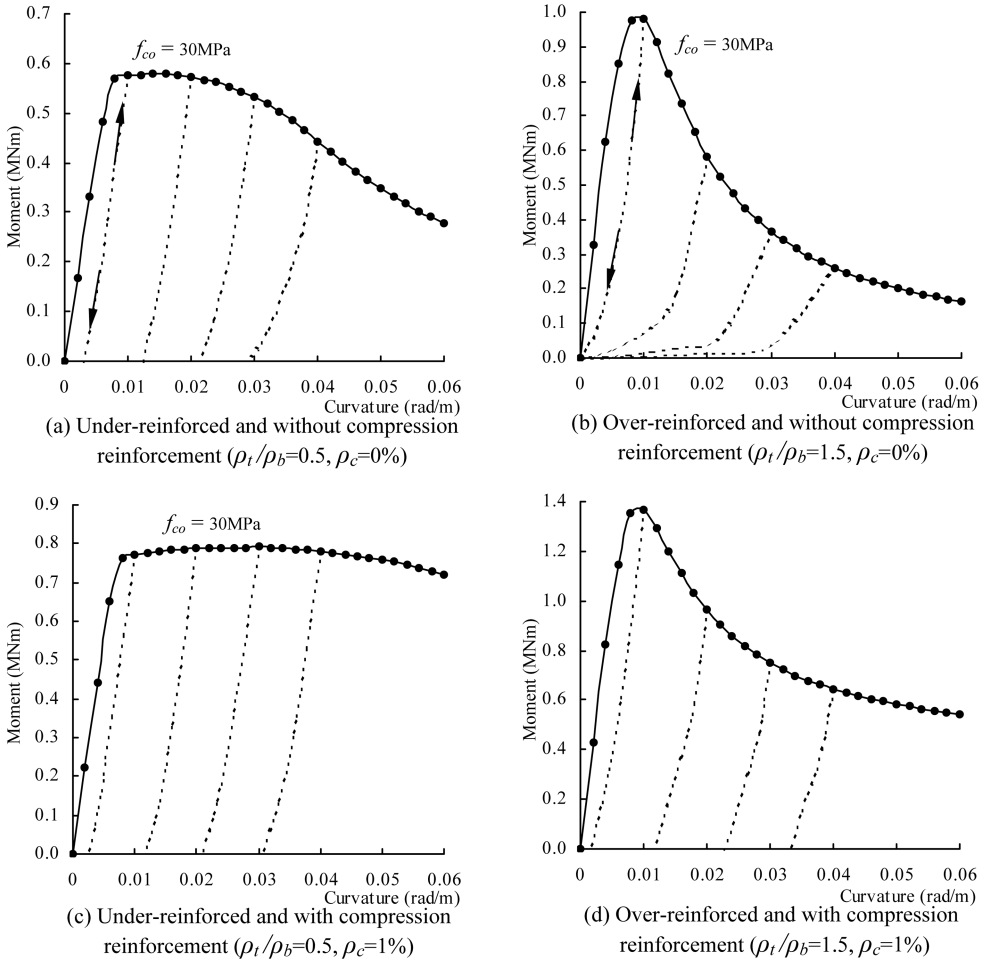

(a) Under-reinforced and without compression reinforcement (ρ_t/ρ_b=0.5, ρ_c=0%)

(b) Over-reinforced and without compression reinforcement (ρ_t/ρ_b=1.5, ρ_c=0%)

(c) Under-reinforced and with compression reinforcement (ρ_t/ρ_b=0.5, ρ_c=1%)

(d) Over-reinforced and with compression reinforcement (ρ_t/ρ_b=1.5, ρ_c=1%)

Fig. 4 Complete moment-curvature relationship of some sections with *in situ* concrete strength 30 MPa

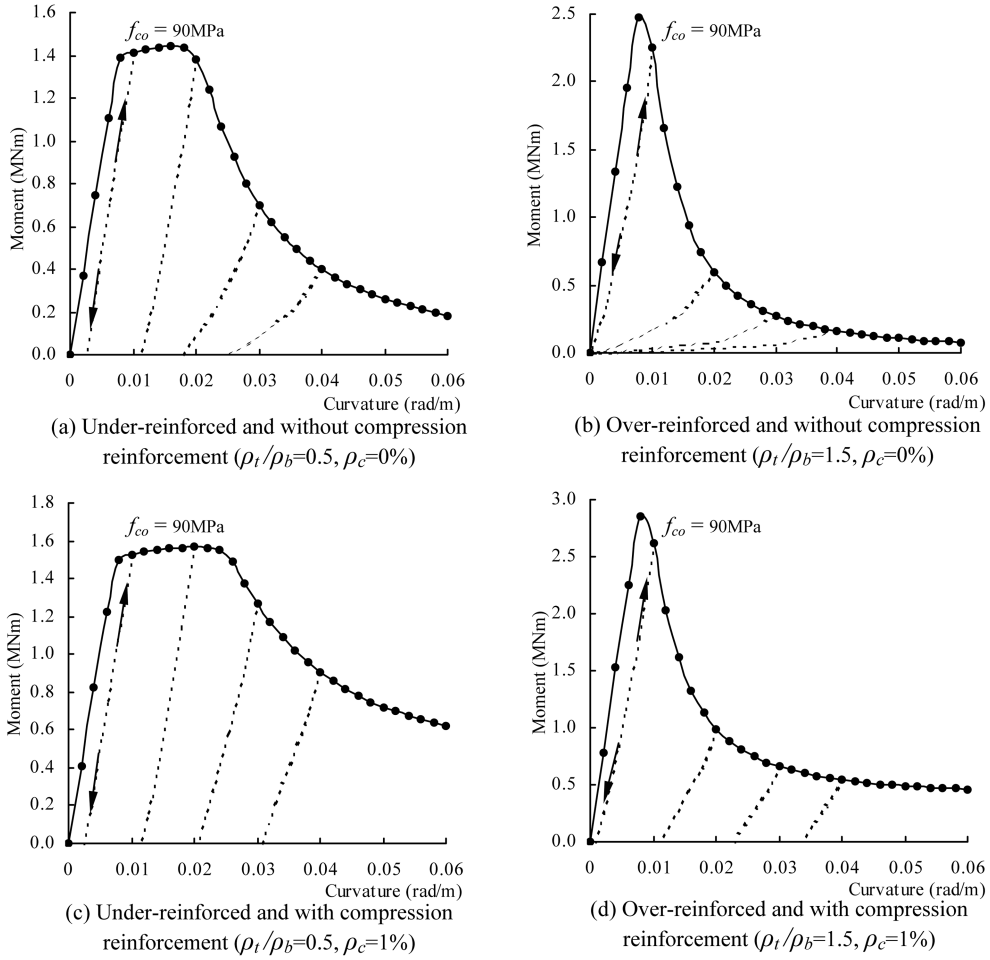

Fig. 5 Complete moment-curvature relationship of some sections with *in situ* concrete strength 90 MPa

assumptions, the complete moment-curvature relationship is moment-path dependent, which is similar to the stress-path dependence of material stress-strain relationship. The envelope of moment-curvature relationship of a beam section experiencing complex load history is the same as the moment-curvature relationship under monotonic loading. The paths of unloading and reloading within the moment-curvature envelope are the same but the paths are slightly curved in most cases. As observed in Figs. 4 and 5, the moment-curvature envelopes in general reflect the ductility of the section examined. In other words, under-reinforced sections are more ductile. The initial portion of the moment-curvature curve is fairly linear followed by a flat plateau that depends on its degree of being under-reinforced. Over-reinforced sections are characterized by sharp peaks in their moment-curvature curves indicating their brittleness.

Fig. 6 summarizes the normal response of beam sections experiencing complex load history. When the curvature increases from zero, the moment-curvature relationship follows path 0-1-3 initially. On unloading from point 3, it follows path 3-2. Upon reloading from point 2, it goes along path 2-3-4-6. The response along path 2-3 is elastic but not perfectly linear. Unloading at small

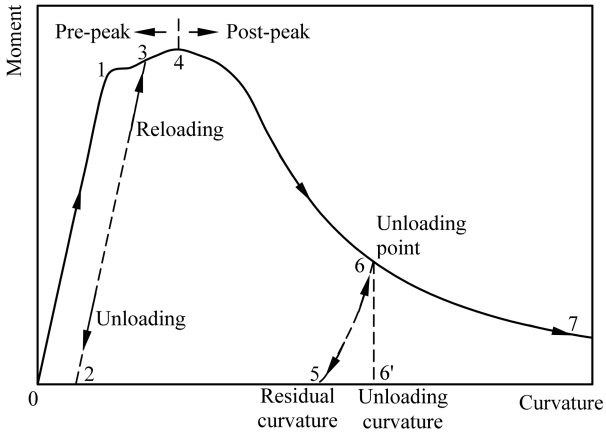

Fig. 6 General view of complete moment-curvature relationship of a typical beam section experiencing complex load history

curvatures before reaching the peak moment is normally along a path broadly parallel to the initial tangent at the origin resulting in small residual curvatures. However unloading at large curvatures after reaching the peak moment is along paths at reduced inclinations suggesting increasing deterioration in stiffness. Such deterioration in stiffness is particularly noticeable in over-reinforced sections without compression reinforcement as in Figs. 4(b) and 5(b).

5.3. Variation of neutral axis depth

The variations of the neutral axis depth d_n for sections with *in situ* concrete compressive strength f_{co} of 60 MPa are plotted in Fig. 7, where the solid lines denote the loading curves and the dash lines stand for the paths for unloading and reloading. The variations for under- and over-reinforced

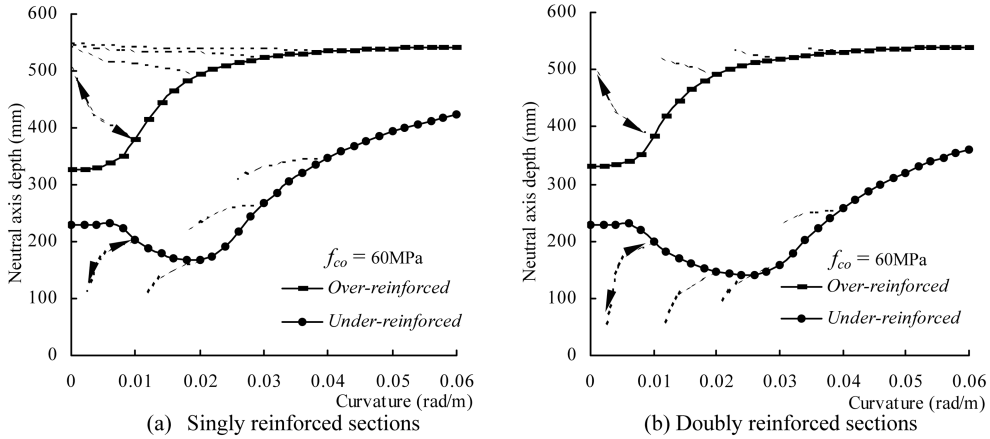

(a) Singly reinforced sections (ρ_t/ρ_b=0.5 and 1.5, ρ_c=0%)

(b) Doubly reinforced sections (ρ_t/ρ_b=0.5 and 1.5, ρ_c=1%)

Fig. 7 Variation of neutral axis depth of sections with *in situ* concrete strength 60 MPa

sections are markedly different but the presence or not of compression reinforcement is immaterial. For both under- and over-reinforced sections, the neutral axis depths remain nearly constant initially. As the curvature increases more, for the under-reinforced sections, the neutral axis depth decreases and then increases as the bending moment enters the post-peak stage. However, for the over-reinforced sections, the neutral axis depth keeps on increasing with curvature.

The difference between under- and over-reinforced sections is again observed in the variation of neutral axis depth upon unloading and reloading. When under-reinforced sections are unloaded, the neutral axis depth keeps decreasing with the curvature. On the contrary, when over-reinforced sections are unloaded, the neutral axis depth increases as the curvature decreases. Similar phenomena are also observed in the sections with *in situ* concrete compressive strength f_{co} of 30 and 90 MPa.

5.4. Residual curvature

It can be observed from Figs. 4 and 5 that there are residual curvatures in most cases when the

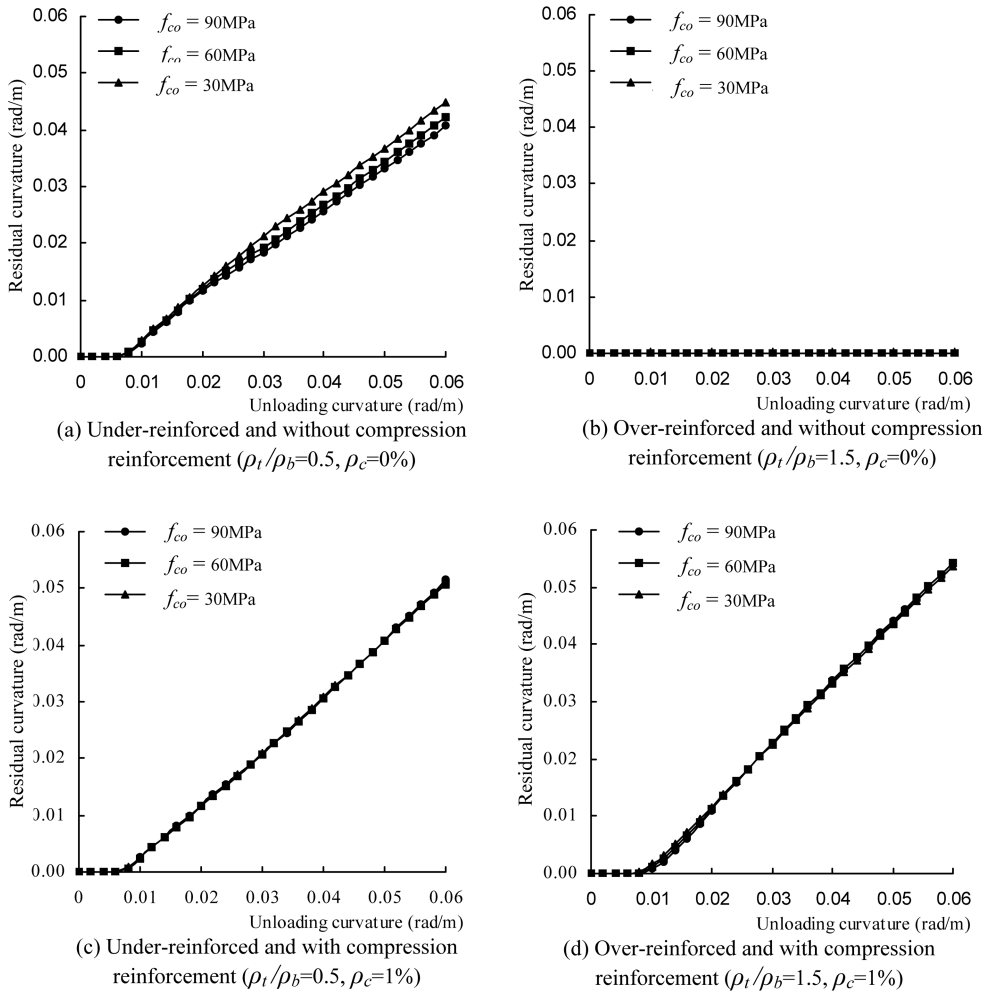

(a) Under-reinforced and without compression reinforcement (ρ_t/ρ_b=0.5, ρ_c=0%)

(b) Over-reinforced and without compression reinforcement (ρ_t/ρ_b=1.5, ρ_c=0%)

(c) Under-reinforced and with compression reinforcement (ρ_t/ρ_b=0.5, ρ_c=1%)

(d) Over-reinforced and with compression reinforcement (ρ_t/ρ_b=1.5, ρ_c=1%)

Fig. 8 Residual curvatures after unloading

applied bending moment is removed. Notable exceptions are over-reinforced sections without compression reinforcement, which result in very small residual curvatures even when unloaded from very large curvatures, as shown in Figs. 4(b) and 5(b). Fig. 8 shows the relationship between residual curvatures and the maximum curvatures from which unloading starts. The behavior of the sections is essentially elastic when the applied curvature is small, and therefore there is effectively no residual curvature. Beyond a certain applied curvature, the residual curvature roughly increases linearly with the applied curvature. Moreover the residual curvature is not much affected by the concrete grade used. The residual curvatures of over-reinforced sections without compression reinforcement are virtually zero. It is noted that the residual curvatures are predominantly caused by plastic strains in the steel reinforcement. For over-reinforced sections without compression reinforcement, the steel reinforcement remains elastic throughout and that explains why the residual curvatures are very small.

5.5. Stress distribution in beam section

The concrete stress distributions of sections with *in situ* concrete compressive strength f_{co} of 60 MPa are shown in Fig. 9. Around the curvature where the peak moment is developed, the concrete

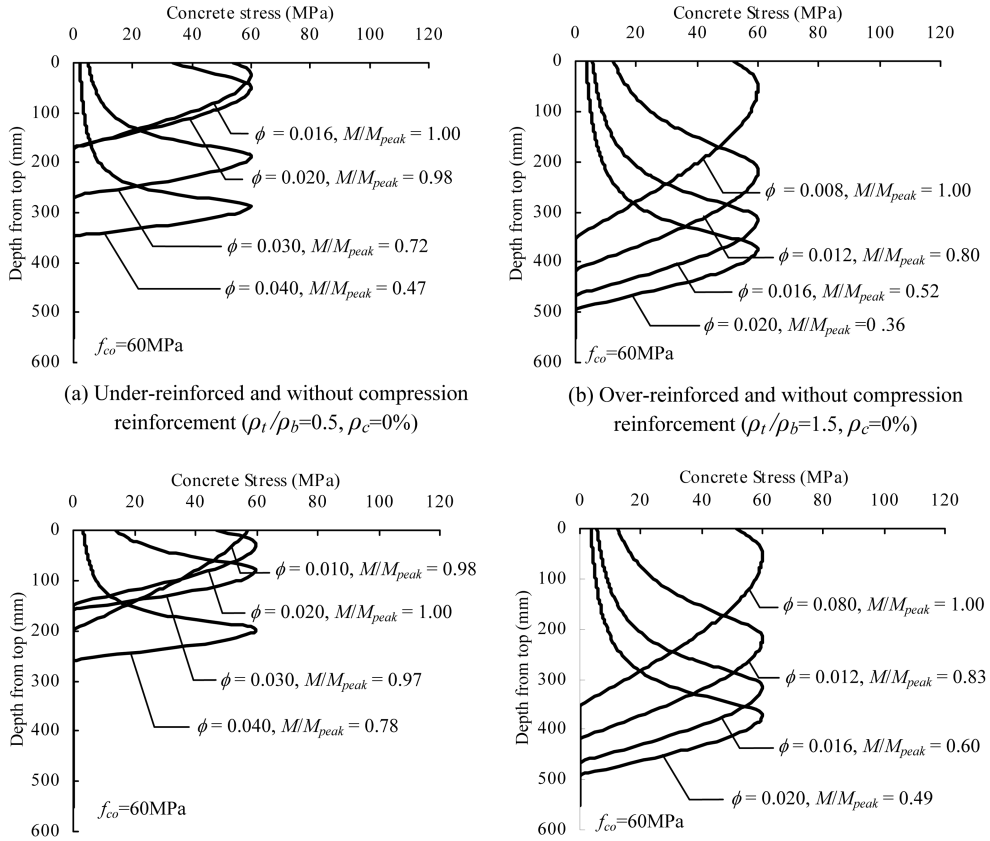

(a) Under-reinforced and without compression reinforcement (ρ_t/ρ_b=0.5, ρ_c=0%)

(b) Over-reinforced and without compression reinforcement (ρ_t/ρ_b=1.5, ρ_c=0%)

(c) Under-reinforced and with compression reinforcement (ρ_t/ρ_b=0.5, ρ_c=1%)

(d) Over-reinforced and with compression reinforcement (ρ_t/ρ_b=1.5, ρ_c=1%)

Fig. 9 Concrete stress distributions of sections with *in situ* concrete strength 60 MPa at different curvatures

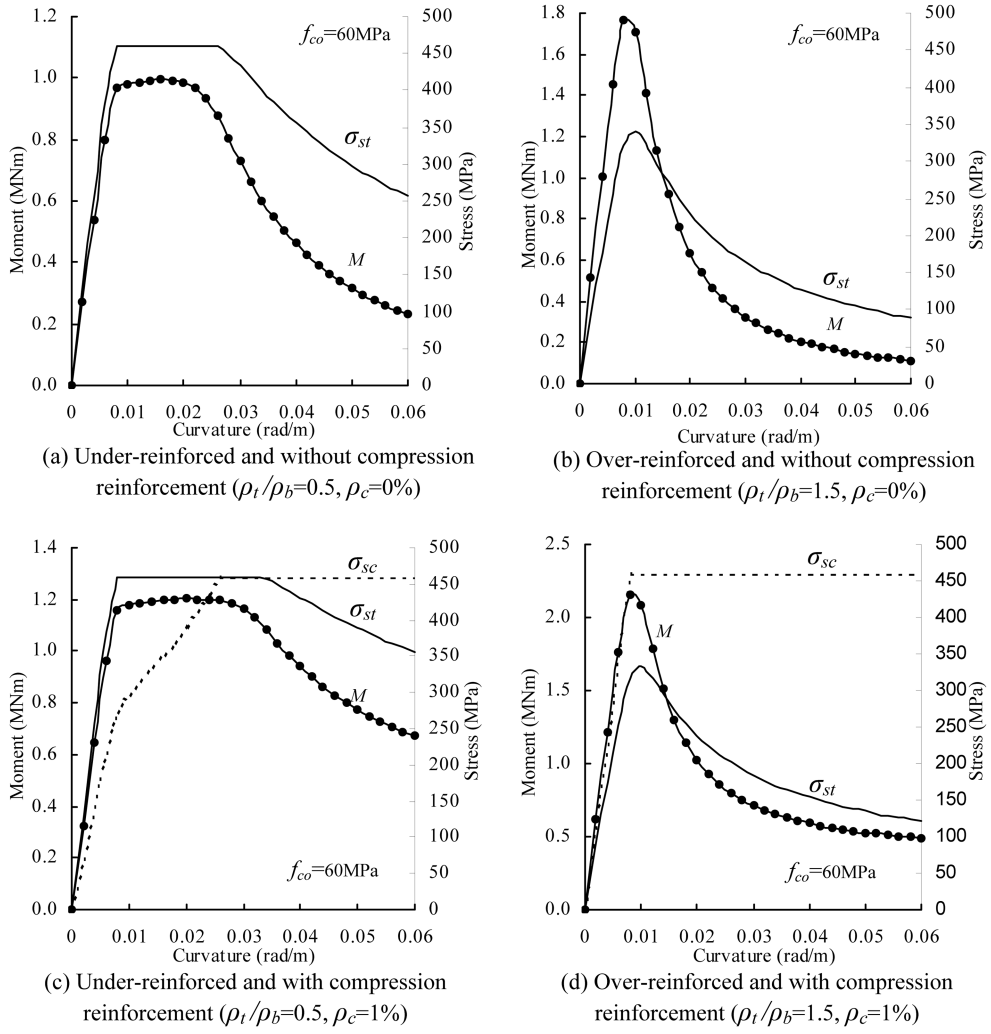

(a) Under-reinforced and without compression reinforcement (ρ_t/ρ_b=0.5, ρ_c=0%)

(b) Over-reinforced and without compression reinforcement (ρ_t/ρ_b=1.5, ρ_c=0%)

(c) Under-reinforced and with compression reinforcement (ρ_t/ρ_b=0.5, ρ_c=1%)

(d) Over-reinforced and with compression reinforcement (ρ_t/ρ_b=1.5, ρ_c=1%)

Fig. 10 Variation of steel stresses and moment with curvature for sections with *in situ* concrete strength 60 MPa

stress distribution has roughly a parabolic shape. The major difference between under- and over-reinforced sections is that, for over-reinforced sections, there is more rapid downward shift in the position of the stress peaks accompanied by more drastic decrease in resisting moment. The variations of steel stresses are plotted against the curvature together with the resisting moment in Fig. 10. It is seen that for under-reinforced sections, the tension reinforcement yields around the peak moment, while the tension reinforcement in over-reinforced sections never yields. Because of the strains imposed, the compression reinforcement always yields if provided. At the post-peak stage when the resisting moment decreases with increasing curvature, the stress in tension reinforcement decreases indicating stress reversal clearly.

The changes in stress distribution on unloading are also investigated. Fig. 11 shows the stresses of the doubly reinforced sections with *in situ* concrete compressive strength f_{co} of 90 MPa at several stages of unloading. It can be seen that although the peak concrete stress drops, the position of the

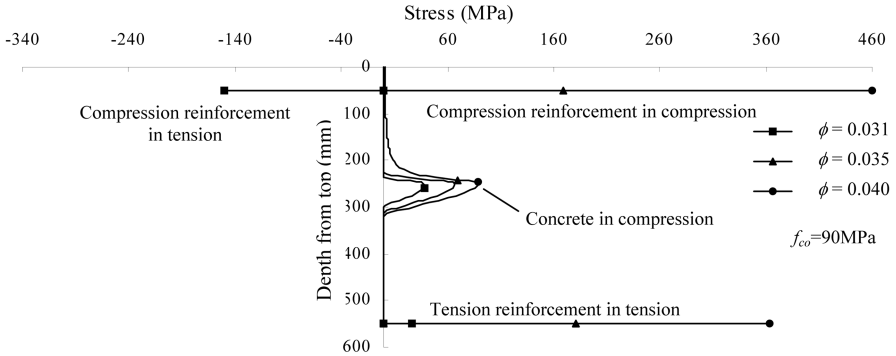

(a) Under-reinforced section unloaded from curvature 0.040
(ρ_t/ρ_b=0.5, ρ_c=1%, residual curvature = 0.031)

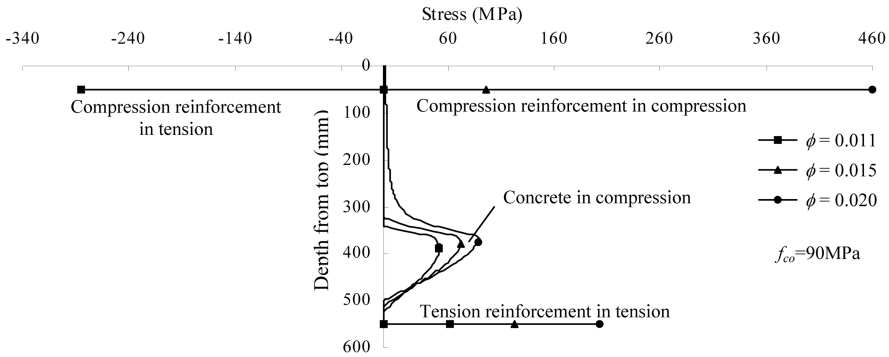

(b) Over-reinforced section unloaded from curvature 0.020
(ρ_t/ρ_b=0.5, ρ_c=1%, residual curvature = 0.011)

Fig. 11 Stress distributions of doubly doubly reinforced sections with *in situ* concrete strength 90 MPa during unloading

peak does not vary much. The stress in tension reinforcement decreases with curvature resulting in some residual tensile stress after complete unloading. The stress in compression reinforcement also decreases with curvature but the residual stress after complete unloading becomes tensile. After the complete unloading, concrete still carries some compressive stress while the top and bottom reinforcing bars all carry tensile stresses. The residual stresses are not significant in sections made of concrete of low strength, and they tend to increase with the concrete grade.

5.6. Strain energy density of beam section

When a beam is loaded, it will deform. The work done by the external load should be equal to the strain energy stored in it. The strain energy density U_0 of a beam section is defined here as the strain energy per unit length of the beam. For convenience, the strain energy induced by shear and axial forces is neglected. Therefore the strain energy density U_0 can be written as

$$U_0 = \int_{LoadingPath} M(\phi)d\phi \tag{12}$$

where the integral should be evaluated along the moment-path. Referring to Fig. 6, the strain energy

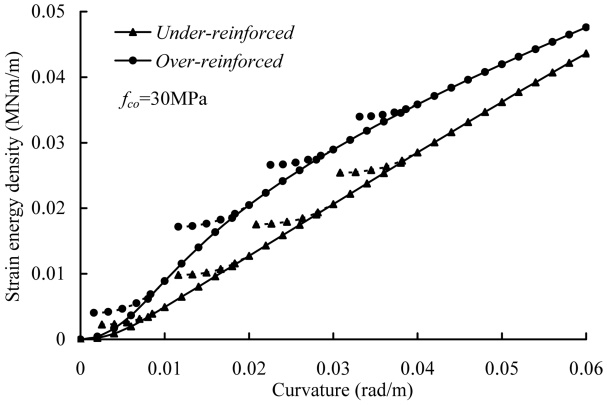

Fig. 12 Strain energy densities of doubly reinforced sections with *in situ* concrete strength 30 MPa under complex load history

density U_0 at point 6 is equal to the area bounded by 0-2-5-6'-6-4-3-1-0. The strain energy stored in a section comprises the elastic and plastic components. While the elastic component can be released with unloading, the plastic component still remains. If the section is unloaded from point 6 to point 5, the strain energy density U_0 becomes equal to that at point 6 minus the elastic component that is the area bounded by 5-6'-6-5. The strain energy densities of the doubly reinforced sections with *in situ* concrete compressive strength f_{co} of 30 MPa are plotted in Fig. 12. The solid lines denote the results for loading while the dash lines denote those for unloading. It is noted that comparatively the under-reinforced section dissipates energy in a more uniform manner because of the yielding of tension reinforcement. Unloading only recovers a small part of the strain energy stored.

5.7. Post-peak behavior of structures considering moment-path dependence

Experiments to investigate the full-range behavior of RC beams upon monotonic imposition of displacement have to be conducted in the displacement-control mode so that the post-peak performance can be observed. For simplicity, a simply supported beam is taken as an example for discussion. Before the peak strength of the beam is reached (i.e. at the pre-peak stage), the curvatures of all sections increase although at different rates. When the peak strength of a beam is reached, the critical section of the beam and its vicinity will reach their respective peak strength and enter the post-peak stage. At the post-peak stage of the critical section when the resisting moment at the critical section drops, equilibrium of the beam requires that the bending moments elsewhere should decrease as well. The sections other than those in the vicinity of the critical section will undergo unloading and release part of their strain energy stored as they are still at the pre-peak stage. The strain energy released by the unloading sections will be absorbed by those in the vicinity of the critical section forming a plastic hinge.

The numerical analysis of the full-range behavior of a beam is much more complicated than that of its sections. Before the peak strength of the beam is reached, the resisting moment at a typical section increases with its curvature and vice versa. After reaching the peak strength of the beam, the resisting moment at the critical section or plastic hinge decreases while its curvature increases. In other words, it follows the envelope curve of the moment-curvature diagram. Therefore the critical section has positive tangent stiffness at the pre-peak stage, but negative tangent stiffness at the post-peak stage.

At the post-peak stage of the critical section when its resisting moment drops, equilibrium of the beam requires that the bending moments elsewhere should decrease as well. Sections carrying moments much lower than the peak moment are clearly at the pre-peak stage and will start unloading. However when the critical section reaches its peak moment, those in the vicinity also carry moments close to the peak moment. As the critical section enters the post-peak stage, the drop in bending moment in the vicinity may encounter some kind of bifurcation, as it may be associated with further increase in curvature or reduction in curvature. The further increase in curvature will follow the post-peak branch of the envelope and therefore has a negative tangent stiffness. On the other hand, the reduction in curvature will follow an unloading path and has a positive tangent stiffness. Apart from the equilibrium, compatibility and energy considerations will come into play in deciding which path the section follows. More work in this direction is necessary to quantify the post-peak behavior of RC beams.

6. Conclusions

The moment-curvature relationship of reinforced concrete beams made of normal- and high-strength concrete experiencing complex load history is studied using a numerical method that employs the actual stress-strain curves of the constitutive materials and takes into account the stress-path dependence of the concrete and steel reinforcement. The effects of loading, unloading and reloading have been studied. The reinforced concrete beam sections studied cover normal- and high-strength concrete, singly and doubly reinforced sections, and under- and over-reinforced sections. The results show that the complete moment-curvature relationship is also path-dependent, which is similar to the material stress-strain relationship with stress-path dependence. However, the unloading part of the moment-curvature relationship of the beam section is elastic but not perfectly linear, although the unloading of both concrete and steel is assumed to be linearly elastic. Unloading from large curvatures normally follows paths with reduced inclinations compared with the initial tangent at origin, suggesting increasing deterioration in stiffness. It is also observed that when unloading happens, the variation of neutral axis depth has different trends for under- and over-reinforced sections. Moreover, even when the section is fully unloaded, there are still residual curvature and stress in the section in some circumstances. It is noted that the residual curvatures are predominantly caused by plastic strains in the steel reinforcement. For over-reinforced sections without compression reinforcement, the steel reinforcement remains elastic throughout resulting in very small residual curvatures. The strain energy densities of different sections are studied. Various issues related to the post-peak behavior of reinforced concrete beams have also been discussed.

References

ACI Committee 363 (1992), *State-of-the-art report on high strength concrete*, ACI 363-R92, American Concrete Institute, Detroit, U.S.A.

Attard, M. M. and Setunge, S. (1996), "The stress-strain relationship of confined and unconfined concrete", *ACI Mater. J.*, **93**(5), 432-442.

Au, F. T. K. and Kwan, A. K. H. (2004), "A minimum ductility design method for non-rectangular high-strength concrete beams", *Comput. and Conc., An Int. J.*, **1**(2), 115-130.

Bangash, M. Y. H. (2001), *Manual of Numerical Methods in Concrete: Modelling and Applications Validated by*

Experimental and Site-Monitoring Data, Thomas Telford Ltd, London, U.K.
Brown, R. H. and Jirsa, J. O. (1971), "Reinforced concrete beams under load reversals", *ACI J.*, **68**(5), 380-390.
Carreira, D. J. and Chu, K. H. (1986), "The moment-curvature relationship of reinforced concrete members", *ACI J.*, **83**(2), 191-198.
Gerald, C. F. and Wheatley, P. O. (1999), *Applied Numerical Analysis*, 6th Ed., Addison-Wesley, USA, 698pp.
Kent, D. C. and Park, R. (1971), "Inelastic behavior of reinforced concrete members with cyclic loading", *Bulletin of New Zealand Society of Earthquake Engineering*, **4**(1), 108-125.
Kwan, A. K. H. and Au, F. T. K. (2004), "Flexural strength-ductility performance of flanged beam sections cast of high-strength concrete", *The Structural Design of Tall Buildings*, **13**(1), 29-43.
Pam, H. J., Kwan, A. K. H. and Ho, J. C. M. (2001), "Post-peak behavior and flexural ductility of doubly reinforced normal- and high-strength concrete beams", *Struct. Eng. and Mech.*, **12**(5), 459-474.

Notation

A_{sc} = area of compression reinforcement
A_{st} = area of tension reinforcement
b = breadth of rectangle beam section
d = depth to centroid of tension reinforcement
d_1 = depth to centroid of compression reinforcement
d_n = neutral axis depth
E_c = Young's modulus of concrete
E_s = Young's modulus of steel reinforcement
f_{ci} = stress at inflection point on descending branch of stress-strain curve of concrete
f_{co} = in situ uniaxial compressive strength of concrete
f_y = yield strength of steel reinforcement
h = total depth of the beam section
x = distance above neutral axis
ε = strain in section
ε_c = strain in concrete
ε_{ce} = compressive strain at extreme compression fibre of concrete
ε_{ci} = strain at inflection point on descending branch of stress-strain curve of concrete
ε_{co} = strain in concrete at peak stress
ε_{pc} = residual plastic strain in concrete
ε_{ps} = residual plastic strain in steel reinforcement
ε_s = strain in steel reinforcement
ε_{sc} = compressive strain in compression reinforcement
ε_{st} = tensile strain in tension reinforcement
ε_y = yield strain of steel reinforcement
ρ_b = balanced steel ratio of beam section
ρ_c = compression steel ratio (= A_{sc}/bd)
ρ_t = tension steel ratio (=A_{st}/bd)
σ_c = stress in concrete
σ_s = stress in steel reinforcement
ϕ = curvature of beam section

CC